Characterization of TiAlSiN/TiAlSiON/SiO_2 optical stack designed by modelling calculations for solar selective applications

L. Rebouta[1*], P. Capela[1], M. Andritschky[1,2], A. Matilainen[2], P. Santilli[2], K. Pischow[2] , E.Alves[3]

1 Centre of Physics, University of Minho, Azurém, 4800-058 Guimarães, Portugal

2 Savo Solar Oy, Insinöörinkatu 7, 50100 Mikkeli, Finland

3 ITN, Physics Department, EN. 10, 2686-953 Sacavém, Portugal

* Corresponding author: Tel.: +351 253510472; fax: +351 253510461, e-*mail address*: rebouta@fisica.uminho.pt

Abstract

Preparation and characterization of TiAlSiN/TiAlSiON/SiO_2 solar selective absorber is reported in this contribution. All layers were deposited in a continuous mode using a industrial equipment, the nitride and oxynitride were prepared by reactive magnetron sputtering and the SiO_2 layer by Plasma Enhanced Chemical Vapor Deposition. The optical constants of individual layers were calculated by modelling of spectral transmittance and reflectance of the individual layers. The three layer stack absorber was then designed using those optical properties. The thickness of the individual layers was optimized until a solar absorptance of 96% was obtained resulting in a total thickness of about 200 nm, deposited in copper and extruded aluminium absorbers. A thermal emittance of 5 % for an absorber temperature of 100 ºC was obtained by analyzing the measuring data from a FTIR spectrometer with integrating sphere. After test duration of 600 h, the samples subjected to a thermal annealing at 278 ºC in air showed a performance criterion (PC) below 4% for, while the samples in the humidity tests showed a PC below 2 %,

Keywords: TiAlSiN; TiAlSiNO; SiO_2; solar selective absorber, dielectric function modelling

1. Introduction

The goal of the solar selective absorber is to maximize the absorption in the visible and near infra-red light wavelength region and minimize the thermal emittance in the deep infrared region [1]. The most commonly used design is based on a selectively solar-absorbing and infrared transparent layer on top of a substrate that has high infrared reflectance. The base material of solar absorbers is often a metal with high thermal conductivity such as copper or aluminium.

A very high solar absorption can be achieved when the coating has a graded refractive index and extinction coefficient, which should be highest closest to the metal substrate (infrared reflector) and then gradually decreasing towards the surface. A destructive interference is created in the visible spectrum, which can increase the solar absorption to 98%. This continuously decreasing can be

simplified by the use of few layers (2–5 layers) with decreasing refractive index namely multilayer gradient coating [2,3], cermets composite coating [4,5] and optical interference coating [6,7]. The design of these multilayered coatings for selective solar absorbers requires a detailed knowledge of the optical constants of the considered materials.

Some transition metal nitrides have shown high chemical stability, high degree of spectral selectivity and also have improved oxidation resistance [8, 9], namely TiN and TiAlN, which have been used in the development of spectrally selective solar absorber [6-8,10-11]. The use oxynitrides has some advantages, not only in logistic terms because allows the use of same targets, but also because the transition metal oxynitrides have good properties for these applications [12] and can be combined with the nitrides. The so-called nanocomposite films, consisting of nanocrystalline transition metal nitrides, MeN, and amorphous Si_3N_4 phase, which have unique mechanical, chemical and tribological properties, have been one of the most promising superhard materials [13-15]. Al addition to these coatings showed promising results, improving the oxidation resistance, thermal stability and the performance in cutting tests [16-18].

Within the frame of this work, an optical stack TiAlSiN/TiAlSiNxOy/SiO_2 was designed and deposited on copper and aluminium. The optical constants of the studied materials have been calculated using the SCOUT software [19] which makes the theoretical analysis of transmittance and reflectance of films. Those optical constants were then used to design the 3 layered stacks for a solar selective absorber.

2. Experimental details

2.1 Sample preparation and characterization

TiAlSiN and TiAlSiNxOy thin films were deposited by dc magnetron sputtering on glass, copper and extruded aluminum (extruded HyLive™ Solar, MPE) substrates, under an Ar/N_2/O_2 atmosphere from a TiAlSi planar target in a continuous mode using a industrial equipment at Savo Solar Oy, with magnetrons with a dimension of 3.2 m x 0.3 m x 0.1 m and having a base pressure of $6x10^{-4}$ Pa. Nitride films were prepared with a variation of the nitrogen gas flow (100 – 156 sccm) and oxynitride films with a variation of nitrogen (150 – 210 sccm) and oxygen flow (90 – 108 sccm) while argon flow was kept constant, whose details are presented in table I. The SiO_2 layer was also deposited in continuous mode by Plasma Enhanced Chemical Vapor Deposition (PECVD) using a Inductively Coupled Plasma (ICP) source and it was used the Octamethylcyclotetrasiloxane (OMCTS), $((CH_3)_2SiO\text{-})_4$, as a precursor. During those depositions a rf power of 3000 W, an oxygen flow of 750 sccm and precursor flow of 15 g/h were used. The total pressure during deposition was 0.7 Pa.

The structural properties of the films were studied by X-ray diffraction (XRD) employing a Bruker AXS Discover D8 operating with CuKα radiation. X-Ray diffraction measurements have been performed for an angle of incidence of 1º. Optical measurements, in transmittance and reflectance modes, were performed in the wavelength range of 250-2500 nm, using a Shimadzu spectrometer. The reflectance measurements were performed with an incidence angle of 8º using an integrating sphere attachment. A Fourier Transform Infrared (FTIR) spectrophotometer was used to cover the infrared wavelength range, 2.5-16 μm, which is equipped with an integrating sphere. The emissivity was also measured with an emissometer AE-AD3 from Devices & Service Company.
Emissivity is a weighted fraction between emitted radiation and the Planck black body distribution at 100 ºC and the normal solar absorptance, α_{sol}, is defined as a weighted fraction between absorbed radiation and incoming solar radiation [20]. The solar spectrum, used here is defined according to the ASTM G173-03 Reference Spectra. The accelerated life-time testing were performed accordingly the principles presented in ref [21]. A performance criterion (PC) was defined, which can be used to describe the influence of the changes in the solar absorptance (Δα) and the thermal emittance (Δε), on the solar fraction:

$$PC = \Delta\alpha - 0.5\Delta\varepsilon \quad (1)$$

with Δα= α(unaged)- α(after testing) and Δε= ε (unaged)- ε(after testing).
In this definition, a value of the performance criterion of 0.05 corresponds to a relative decrease of the annual solar fraction of a typical domestic hot water system by 5%. The thermal load of solar absorber coating is related with operating temperature, which depends on the solar absorptance and emittance values in a single glazed flat plate solar thermal collector.

2.2 Dielectric function model

The experimental transmittance and reflectance curves were modelled by a commercial optical simulation program (SCOUT) [19] and the thickness and dielectric function of the different layers were calculated. This software uses the classical theory of optical propagation, where atoms or molecules are modelled as classical dipole oscillators and the light is treated as electromagnetic wave. This model assumes that there are several different types of oscillators, each with their own characteristic resonant frequency, and enables the calculation the frequency dependence of the complex dielectric constant, $\tilde{\varepsilon}_r = \varepsilon_1 + i\varepsilon_2$, which can be used to obtain the optical constants, n and κ, being n the normal refractive index and κ the extinction coefficient. This is performed though the relation between the complex dielectric constant and the complex refractive index, $\tilde{n}^2 = \tilde{\varepsilon}_r$, where the complex refractive index is usually defined as $\tilde{n} = n + i\kappa$ [22, 23]. The microscopic response of the material is determined primarily by the polarization and it was assumed that the polarization

varies linearly with electric field strength. The polarization P induced by an externally applied electric field E in a homogeneous material is given by the electric susceptibility , χ, which is closely related to the susceptibility [23]. It was also assumed that the medium is isotropic and uniform, i.e., they have completely smooth and parallel surfaces.

The dielectric function of TiAlSiN, TiAlSiNxOy and SiO_2 was considered as a contribution of intraband and interband transitions and was treated as the sum of the following terms:

$$\tilde{\varepsilon}_r = \tilde{\varepsilon}_{background} + \tilde{\varepsilon}_{Drude} + \sum \tilde{\varepsilon}_{Lorentz} + \tilde{\varepsilon}_{OJL} \quad (2)$$

The Drude term (only used for TiAlSiN films) represents unbound electron oscillators and describes the intraband transitions of the electrons in the conduction band. The Lorentz term represents the bound harmonic oscillators [24] model, which was used to describe the interband transitions into the upper half of the conduction band, and several bound harmonic oscillators were used. The OJL term follows the O'Leary model [25] and was used to describe the band gap transitions for which parabolic bands are assumed with tail states exponentially decaying into band gap. Details about the model and this adaptation can be found in the literature [26]. The parameters used in the fit are the optical band gap energy (Eg), the decay energy, to describe the exponential tail extending into the band gap, and the strength of the transition. Internally, the SCOUT software uses the dielectric function for all computations.

3. Results and discussion

The crystallinity of the samples was investigated by grazing incidence X-ray diffraction analysis. Fig. 1 shows the typical XRD spectra for TiAlSiN and TiAlSiOxNy films grown on copper and aluminium substrates and the XRD pattern of copper and aluminium substrates. The XRD patterns of nitride films deposited on copper (Fig 1a) show some diffraction peaks, which can be indexed with solid solution (Ti,Al)N of the cubic NaCl type structure. In the patterns from oxynitrides can be found the same peaks detected for nitrides, but with lower intensity, indicating that they are less crystalline than the nitrides. A similar behaviour was found for layers deposited on aluminium substrates (Fig 1b).

The optical spectroscopy in both transmittance and reflectance modes was used to characterize the optical properties of the films. Fig. 2 depicts the optical transmittance (Fig 2a) and reflectance (Fig 2b) data for representative nitrides (TiAlSiN) prepared with different N_2 flows and in Fig.3 are displayed the results for representative oxynitrides (TiAlSiNO) prepared with different N_2 and O_2 flows (Fig 3a and 3b), as indicated in the figures. All these layers were deposited on glass using a conveyor speed of 0.70 m/min for nitrides and a conveyor speed of 0.63 m/min for oxynitrides. The different reactive gases flows allowed obtaining a wide range of reflectance and

transmittance values, from which it is possible to select the layers with adequate optical constants and construct the desired optical stack. In Fig.4 are shown the transmittance and reflectance of glass substrate and of two SiO_2 films with different thickness deposited on glass. It is clearly seen the increase of the transmittance (and respective decrease in reflectance) in visible range and in comparison with glass substrate, when is deposited a 60 nm SiO_2 layer on glass.

Experimental curves (T and R) were modelled with SCOUT software [19] by using the model briefly described in section 2.2. The optical constants (refractive index, n, and extinction coefficient, κ) of coatings were calculated for the films deposited on glass, because the optical constants are more accurately calculated when we have information from transmittance and reflectance. Previously to the calculation of the optical properties of the films, reflectance and transmittance of the glass substrate were modelled and its dielectric function was calculated, which was used in the remaining calculations. In case of oxynitrides, the Drude contribution was not used in the already described model. A good agreement between the simulated and experimental data was obtained (simulations are represented in Fig. 2 and 3 by the thin lines) and the obtained refractive index and extinction coefficient are plotted in Fig. 5 as a function of the wavelength and for same samples shown in Fig. 2-4. The thicknesses of those films were obtained from the fit to experimental spectral transmittance and reflectance curves and are indicated in the table I.

In case of nitrides (Fig. 5a), it is observed an increase of refractive index and extinction coefficient with the wavelength, what is a characteristic behaviour of metallic films. It is also seen that the increase of nitrogen flow induces a decrease of both refractive index and extinction coefficient. In the case of oxynitrides (Fig.5b), the optical constants vary from metallic characteristics (O2 sample) to semiconductor behaviour (O4 sample). The refractive index of this film does not show appreciable variation with wavelength and the extinction coefficient reveals a maximum around 1000 nm and then it decreases, which is a behaviour expected for a semiconductor. In this case, a variation of any of the reactive gases (N_2 or O_2) flow results in a variation of the optical constants (refractive index and extinction coefficient). These results are in accordance with the metallic behaviour of these type of nitrides and the semiconducting properties of this family of oxynitrides [27].

The optical constants of SiO_2 are shown in Fig. 5c and as expected, the extinction coefficient of SiO_2 is almost zero, which is consistent with a dielectric behaviour and the refractive index is about 1.45 for wavelengths higher than 500 nm, which makes this material a good antireflection layer. In order to build the 3 layers (TiAlSiN/TiAlSiON/SiO_2) absorber on a copper and aluminium substrates, several simulations were performed using the optical properties of the substrate and different nitrides and oxynitrides. The destructive interference effect can be obtained with different solutions and for a copper substrate can be achieved with the nitride layer with an average refractive

index of about 2.2 and an extinction coefficient around 0.8-1.0 in the wavelength range 500 – 700 nm and increasing for higher wavelengths and with an oxynitride layer with an average refractive index of about 2.3-2.4 and an extinction coefficient below 0.2, without appreciable variation for higher wavelengths. From the simulation using the different nitride and oxynitride layers, the chosen combination for a copper substrate is the following:

TiAlSiN – N2 layer ~53 nm

TiAlSiON – O4 layer ~ 44 nm

SiO_2 ~95 nm

The thickness of the different layers was adjusted by the conveyor speed variation. The calculated reflectance (wavelength range from 0.25 to 2.5 μm) for the best layer combination (solar absorptance of 96%) is shown in Fig. 6 together with the measured reflectance of the corresponding deposited sample (solar absorptance of 95%). The reflectance of the Cu/TiAlSiN/TiAlSiON/SiO_2 optical stack was measured with a UV/Vis/NIR (from 0.25 to 2.5 μm) and a FTIR (wavelength range 2.5 - 16 μm) spectrophotometers. The emissivity was calculated from the reflectance in wavelength range from 2.5 to 16 μm and was obtained an emissivity less than 6% for an absorber temperature of 100 ºC. The emissivities of samples cut from two different absorbers from well known producers were also measured with same procedure and emissivities of 6% and 7% were obtained, respectively.

In order to evaluate the thickness calculation using the modelling software, the same optical stack was deposited in a silicon substrate and analyzed by Scanning Electron Microscopy (SEM) in fractured cross section. A SEM cross-sectional micrograph of TiAlSiN/TiAlSiON/SiO_2 coating is shown in Fig. 7, and the thicknesses of the two first layers (TiAlSiN ~51 nm and TiAlSiON ~40 nm) are very similar to those calculated using SCOUT software. These layers show a columnar growth. From this image was not possible to evaluate the thickness of the SiO_2 layer.

Two types of accelerated life-time tests were performed with samples deposited on copper and aluminium, both with duration of 600 hours. Thermal load tests were performed at a temperature of 278 ºC in air, and humidity test at 40 ºC with 95% of humidity and continuous water condensation on the surface. Several samples were tested and representative results obtained with samples deposited on extruded aluminium (as extruded and furnace brazed) substrates are shown in Fig. 9. Main changes in absorptance (Fig. 9a) happened during the first 36 h of the test, and a very small variation was found between the measurement performed after 36 h and that performed after 600 h, which shows a very good stability. The emissivity does not show appreciable variation (Fig. 9b) during the accelerated life time tests, which indicates that the initial absorptance variation can be due to an oxidation of the outermost layers of the optical stack. The performance criterion (PC), described in section 2.1 (equation 1) and in ref [21], of same optical stacks are shown in Fig. 10. After a test duration of 600 h, the samples subjected to the oxidation resistance tests showed a PC below 4% for, while the samples in the humidity tests showed a PC below 2 %,

which is a good performance for the indicated application. The main variation occurs during the first 36 h of the tests (coming from absorptance variation shown in Fig. 9).

4. Conclusions

Design and deposition of interference coating TiAlSiN/TiAlSiON/SiO2 for selective absorption of solar radiation was performed. The dielectric function and the thickness of the different layers deposited on glass were calculated through the modelling of the experimental transmittance and reflectance curves by a commercial optical simulation program (SCOUT). The optical constants of the individual layers were then used to construct the three layers stack. The as deposited optical stack (on copper and extruded aluminium substrates) revealed an absorptance higher than 95 %and emissivity of about 5 %. These stacks were subjected to accelerated life-time tests (thermal load and humidity) considering an application as in single glazed, flat-plate collectors for domestic hot water systems [21], and the performance criteria was below 4 % for thermal load tests and below 2 % in humidity tests.

Acknowledgements

The authors acknowledge the funding from the Finnish Funding Agency for Technology and Innovation, Tekes, and from FEDER funds through the "Programa Operacional Factores de Competitividade – COMPETE" and from national funds by FCT- "Fundação para a Ciência e a Tecnologia", under project no. PEst-C/FIS/UI0607/2011.

References

1- G.A. Niklasson and C. G. Granqvist, J. Mat. Sci. 18 (1983) 3475.

2- M. Adsten, R. Joerger, K. Järrendahl, and E. Wäckelgård, Solar Energy, 68 (2000) 325.

3- V. Teixeira, E. Sousa, M.F. Costa, C. Nunes, L. Rosa, M.J. Carvalho, M. Collares-Pereira, E. Roman and J. Gago, Thin Solid Films 392 (2001) 320.

4- M. Farooq, M.G. Hutchins, Solar Energy Materials & Solar Cells 71 (2002) 73–83

5- Q. -C. Zhang and D. R. Mills, J. Appl. Phys., 72 (1992) 3013.

6- A. Biswas, D. Bhattacharyya, H.C. Barshilia, N. Selvakumar and K.S. Rajam, Applied Surface Science 254 (2008) 1694.

7- Miao Du, Lei Hao, Jing Mi, Fang Lv, X. Liu, L. Jiang and S. Wang, Solar Energy Materials & Solar Cells 95 (2011) 1193.

8- R. Blickensderfer, D. K. Deardoff and R.L. Lincoln, Solar Energy 19 (1977) 429.

9-F. Vaz, L. Rebouta, M. Andritschky, M.F. da Silva, J.C. Soares, J. Europ. Ceram. Soc. 17 (1997) 1971-77

10- M. Lazarov, P. Raths, H. Metzger and W. Spirkl, J. Appl. Phys. 77 (1995) 2133.

11- L. Rebouta, A. Pitães, M. Andritschky, P. Capela, M.F. Cerqueira, A. Matilainen, K. Pischow, Surf. Coat. Technol., 2011, http://dx.doi.org/10.1016/j.surfcoat.2011.09.003

12- S. Venkataraj, D. Severin, S.H. Mohamed, J. Ngaruiya, O. Kappertz and M. Wuttig, Thin Solid Films 502 (2006) 228.

13-P. Karvankova, H. Männling, Ch. Eggs, S. Veprek, Surf. Coat. Technol. 146–147 (2001) 280

14 - S. Veprek, M.J.G. Veprek-Heijman, Surf. Coat. Technol. 202 (2008) 5063

15-L. Rebouta, C.J. Tavares, R. Aimo, Z. Wang, K. Pischow, E. Alves, T.C. Rojas, J.A. Odriozola, Surf. Coat. Technol. 133-134 (2000) 234-39

16-F. Vaz, L. Rebouta, M. Andritschky, M.F. da Silva, J.C. Soares, Surf. Coat. Technol. 98 (1998) 912-917

17- S. Veprek, H.D. Mannling, M. Jilek, P. Holubar, Mater. Sci. Eng. A 366 (2004) 202

18- S. Carvalho, L. Rebouta, E. Ribeiro, F. Vaz, C.J Tavares, E. Alves, N.P. Barradas, J.P. Riviere, Vacuum 83 (2009) 1206-12

19- W. Theiss, in: M. Theiss (Ed.), SCOUT Thin Film Analysis Software Handbook, Hard-and Software, Aachen, Germany (http://www.mtheiss.com).

20- J.A. Duffie, W.A. Beckman, Solar Engineering of Thermal Processes, Wiley–Interscience, New York, 1991.

21- M. Kohl, M. Heck, S. Brunold, U. Frei and B. Carlsson, Solar Energy Materials & Solar Cells 84 (2004) 275.

22- T.C. Paulick, Appl.Opt 25 (1986) 562.

23- M. Fox, Optical properties of solids, Oxford University Press Inc, New York, 2001.

24- C.C. Kim, J.W. Garland, H. Abad and P.M. Raccah, Phys. Rev. B 45 **(**1992) 11749.

25- S.K. O_Leary, S.R. Johnson and P.K. Lim, J. Appl. Phys. 82 (1997) 3334.

26- H. Weis, T. Muggenburg, P. Grosse, L. Herlitze, I. Friedrich, M.Wuttig, Thin Solid Films, 351 (1999) 184.

27- P. Carvalho, F. Vaz,_L. Rebouta, L. Cunha, C.J. Tavares, C. Moura, E. Alves, A. Cavaleiro, Ph. Goudeau, E.Le Bourhis, J.P. Rivière, J.F. Pierson, O. Banakh, J Appl. Phys. 98 (2005) 023715

Figure captions

Fig. 1 - Grazing incidence X-ray diffraction patterns of: a) Cu substrate and representative nitride and oxynitride layers deposited on Cu substrates; b) Al substrate and representative three layers stack.

Fig. 2- Reflectance (a) and Transmittance (b) of nitrides layers (TiAlSiN) deposited on glass prepared with different flows of nitrogen (the flows and calculated thicknesses are indicated in table I)

Fig. 3 - Reflectance (a) and Transmittance (b) of oxynitrides layers (TiAlSiON) deposited on glass prepared with different flows of nitrogen and oxygen (the flows and calculated thicknesses are indicated in table I).

Fig. 4 - Transmittance and reflectance of glass substrate and of two SiO_2 layers with different thicknesses deposited on glass.

Fig. 5 - Refractive index (n) and extinction coefficient (κ) as a function of the wavelength of: a) nitrides (TiAlN) prepared with different flows of nitrogen; b) oxynitrides (TiAlNxOy) prepared with different flows of nitrogen and oxygen; c) SiO_2 layer.

Fig. 6 - Calculated (wavelength range from 0.25 to 2.5 μm) and measured (from 2.5 - 16 μm) reflectance of TiAlSiN/TiAlSiNO/SiO_2 optical stack deposited on copper.

Fig. 7 - SEM cross sectional image of TiAlSiN/TiAlSiON/SiO_2 deposited on Si substrate

Fig. 8 – Absorptance (a) and emissivity (b) as a function of the duration of accelerated life time tests of optical stacks deposited on extruded aluminium (as extruded and furnace brazed) substrates.

Fig. 9 – Performance criterion as a function of the duration of accelerated life time tests of optical stacks deposited on extruded aluminium (as extruded and furnace brazed) substrates.

Table I – Reactive gas flows (N_2 and O_2) used in the preparation of different individual layers (nitrides and oxynitrides), and respective thicknesses calculated using the modelling software.

Nitride	N_2 flow (sccm)	Thickness (nm)		Oxynitride	N_2 flow (sccm)	O_2 flow (sccm)	Thickness (nm)
N1	100	49.3		O1	150	108	61.4
N2	130	45.6		O2	150	90	56.5
N3	146	46.4		O3	180	90	56.1
N4	156	45.4		O4	210	90	44.2

Fig. 1a

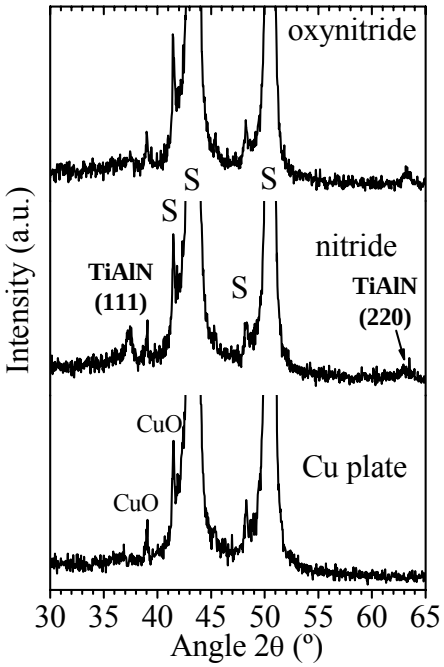

Fig. 1b

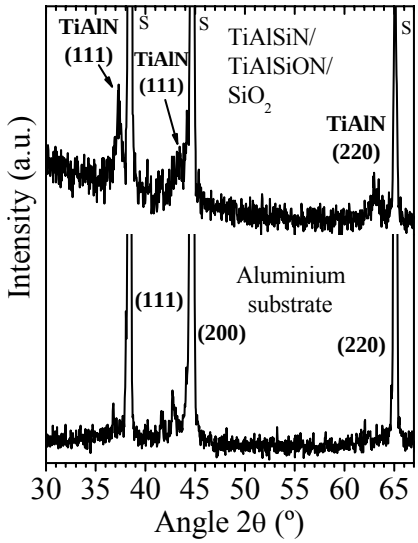

Fig. 2a

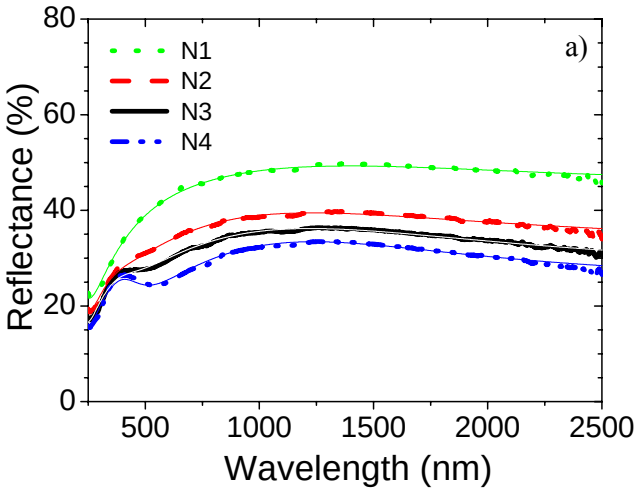

Fig. 2b

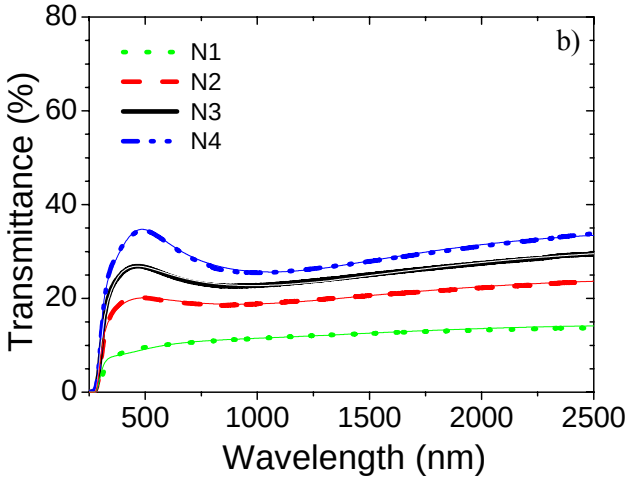

Fig. 3a **Fig. 3b**

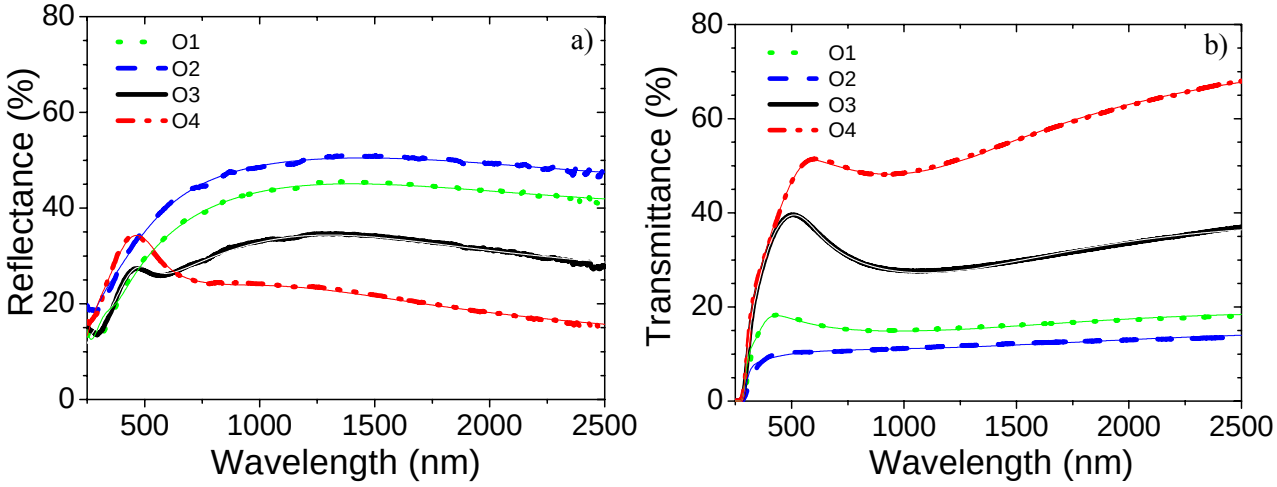

Fig. 4

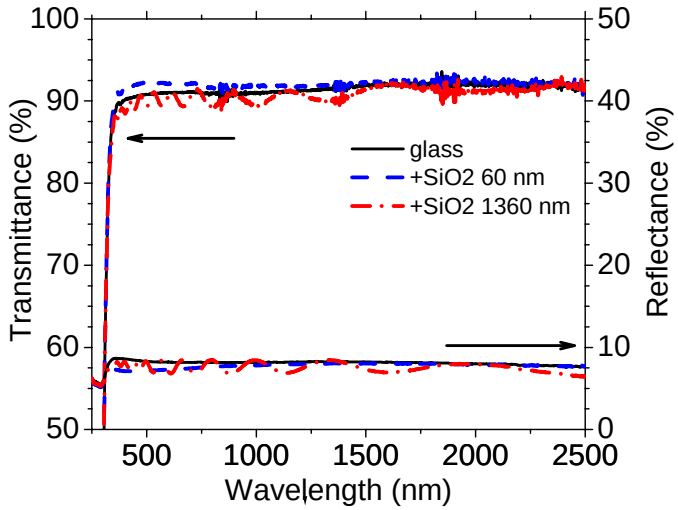

Fig. 5a

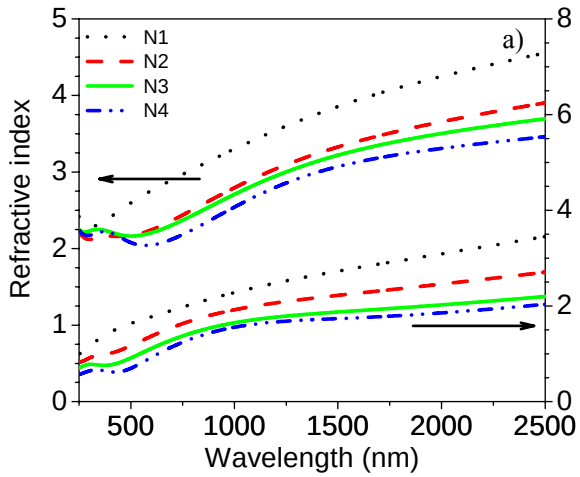

Fig. 5b

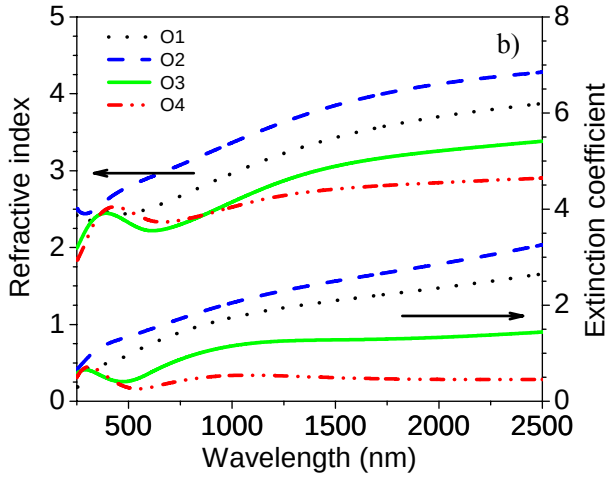

Fig. 5c

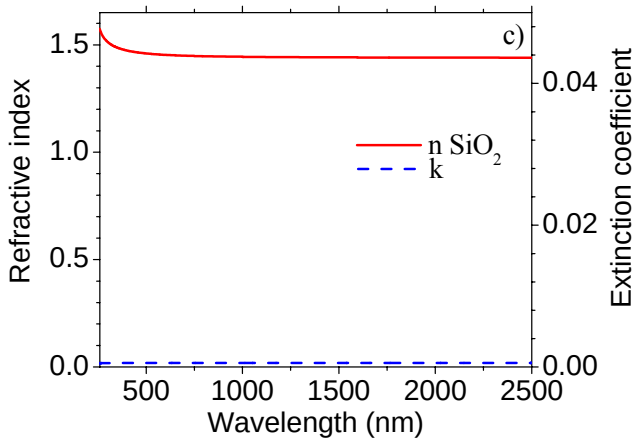

Fig. 6

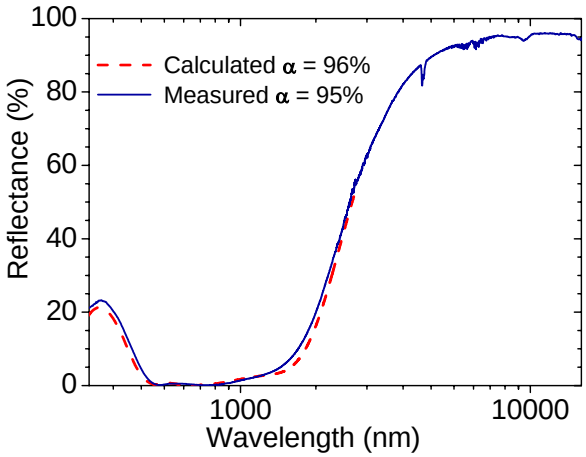

Fig. 7

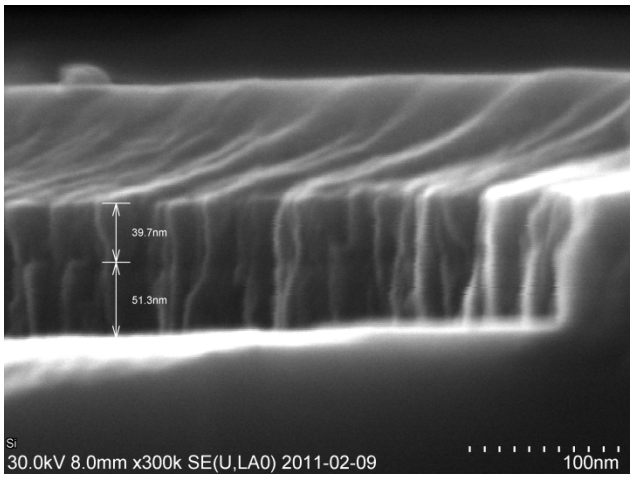

Fig. 8a **Fig. 8b**

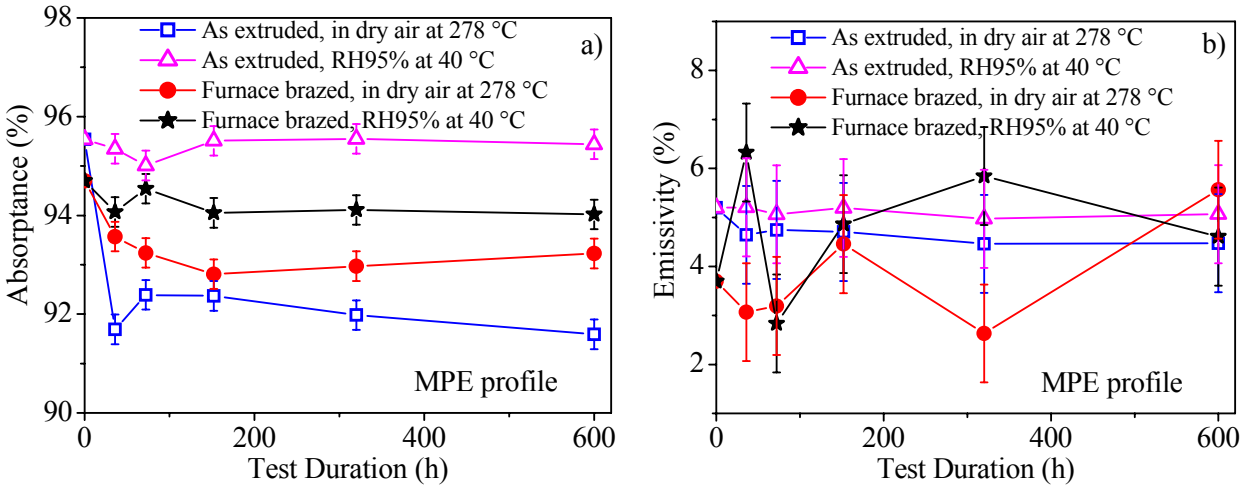

Fig. 9